A molecular dynamics study of the structure of liquid germanium

1989 J. Phys.: Condens. Matter 1 965

(http://iopscience.iop.org/0953-8984/1/5/013)

J. Phys.: Condens. Matter **1** (1989) 965–980. Printed in the UK

A molecular dynamics study of the structure of liquid germanium

A Arnold, N Mauser and J Hafner
Institut für Theoretische Physik, Technische Universität Wien, Karlsplatz 13, A-1040 Wien, Austria

Received 11 July 1988; in final form 26 September 1988

Abstract. The structure of liquid Ge as a function of temperature and density was investigated using molecular dynamics and interatomic forces derived from the pseudopotential theory. We present results for the pair correlation function, the static structure factor and the bond-angle distribution function as a function of temperature and density. Our results are in good agreement with diffraction experiments. The density derivative of the structure factor deviates from the prediction of the uniform-fluid model due to the density dependence of the interatomic potential. The bond-angle distribution shows that the local order in liquid Ge is different from that of both the semiconducting and the metallic crystalline phases. With progressive undercooling the structure of the liquid does not tend towards the structure of amorphous Ge, because solidification is associated with a metal–semiconductor transition resulting in state-dependent interatomic potentials.

1. Introduction

In contrast to most other solids the semiconducting elements Si and Ge and the III–V compound semiconductors like GaAs shrink when they melt [1]. In the crystalline form stable at normal pressures these substances have an open structure with a coordination number four. Diffraction experiments [2–6] show that upon melting the number of nearest neighbours increases to an average value greater than six. The solid–liquid transition is accompanied by a transition from a semiconducting to a metallic state [1]. The metallic melt may be quenched into a semiconducting amorphous state. Under pressure both the amorphous and the crystalline semiconductor transform to a metallic state [7].

The liquid and amorphous forms of Si and Ge have been a subject of extensive theoretical studies [8–18]. Much of the interest has centred around the problem of generating physically reasonable liquid and amorphous structures and to comparing the properties of these structures with experimental results. The attempts to calculate the structures of liquid Si and Ge may be divided into three different classes. The first group of investigations is based on classical potential energy functions including two- and three-body interactions [8–14]. These classical models were developed by fitting to first-principles total-energy calculations for the different polymorphic forms of the crystal and for surface and defect configurations, but it is of course difficult to model all known structural properties. The fundamental work of Car and Parrinello [15, 16] combines

0953-8984/89/050965 + 16 $02.50

quantum-mechanical density functional theory and molecular dynamics in a unified description of the electron–ion system. The third approach is of an intermediate character: linear response theory is used to obtain a systematic decomposition of the potential energy function into a volume term and two- and many-body contributions [17, 18] and these serve as a basis for studies using classical molecular dynamics.

The physical picture emerging from these studies is quite different from that underlying the construction of the classical potential energy functions. In the classical models the potential energy is assumed to consist of two- and three-body contributions ($R_{ij} = |\boldsymbol{R}_i - \boldsymbol{R}_j|$):

$$\Phi(\boldsymbol{R}_i, \ldots, \boldsymbol{R}_N) = \sum_{i<j} \Phi_2(R_{ij}) + \sum_{i<j<k} \Phi_3(R_{ij}, R_{jk}, R_{ki}). \tag{1}$$

The two-body potential $\Phi_2(R)$ is usually assumed to have a deep attractive minimum just at the bond length of the crystalline material [8–10]. If the system were in equilibrium under the action of these pair forces alone, this would result in a very densely packed liquid with coordination numbers around $N_c \simeq 10$–11. In order to reduce the coordination numbers to the value actually observed in liquid Si and Ge, the three-body potential $\Phi_3(R_{12}, R_{13}, \theta)$ (θ is the angle between the vectors $\boldsymbol{R}_{12}$ and $\boldsymbol{R}_{13}$) must be strongly repulsive for small bond angles θ ($\theta \leqslant 70°$), with a minimum close to the tetrahedral angle ($\theta \simeq 110°$–115°). Its form for larger bond angles is evidently less important, it varies considerably among the different models [8–10]. Note that the three-body forces yield a large repulsive contribution to the total energy of the liquid, but only a much smaller one to that of the crystal or the amorphous solid.

From the response theory of the conduction electron gas we learn that the potential energy consists of a volume energy, and electron-density-dependent pair and many-ion terms (n_e is the electron density)

$$\Phi(\boldsymbol{R}_i, \ldots, \boldsymbol{R}_N) = E_1(n_e) + \sum_{i<j} \Phi_2(R_{ij}, n_e) + \sum_{i<j<k} \Phi_3(R_{ij}, R_{jk}, R_{ki}, n_e). \tag{2}$$

It is well known that for all metallic and semiconducting elements and compounds the largest contribution to the total energy comes from the volume term $E_1(n_e)$ [19, 20]. Only for metallic elements with a relatively low electron density the effective interatomic potential Φ_2 has a minimum at the nearest-neighbour distance for close packing. For elements with a higher electron density, the first attractive minimum is progressively covered by the screened interionic repulsions [20, 21]. For Si and Ge this results in an interatomic pair potential, which is repulsive close to the nearest-neighbour distance in a close-packed structure, and has a strong inflection at smaller distances. In that case it will be energetically favourable to distort the nearest-neighbour shell of the close-packed structure in such a way that some of the twelve neighbours are pushed inwards to come to sit close to the depression in the potential, while the remaining atoms are pushed outward towards the minimum. Indeed it is found that the proper coordination number of both the crystalline [21] and the liquid phases [17] follows already from the interplay of the volume and pair forces. Of course this does not mean that three-body forces are unimportant: they influence the triplet correlations, and they are essential for stabilising the low-lying transverse acoustic branches characteristic of the group IV elements in the diamond structure.

In this paper we present an investigation of the structure of liquid and supercooled liquid Ge, based on pseudopotential-derived interatomic forces and molecular dynamics. We find that the structure of liquid Ge is well described on the basis of volume

and pair forces alone; structure factor and pair correlation function agree very well with the available diffraction data. The characteristic features of liquid Ge are drastically sharpened upon supercooling, the structure factor assumes a form intermediate between that of liquid Ge at high temperatures and that of amorphous Ge. However, the bond-angle distribution retains a peak at small bond angles ($\theta \simeq 60°$) which should not exist in semiconducting amorphous Ge. A similar result had been found in molecular dynamics simulations based on the Biswas–Hamann potentials [13]. On the other hand, the small-angle peak is absent in structures generated using the Stillinger–Weber potential [11]. This shows that a classical parametrisation of the interatomic forces is far from unique—even if it is based on an extensive database. Pseudopotential-derived interatomic forces could be a useful starting point for a more realistic approach.

This paper is organised as follows: in § 2 we review very briefly the calculation of the interatomic potentials, details of the molecular dynamics calculations are given in § 3. In § 4 we present the results for liquid and supercooled liquid Ge and we present our conclusions in § 5.

2. Interatomic forces

For simplicity, our calculation of the interatomic forces is based on a simple empty-core pseudopotential—our previous studies of the trends in the crystalline and liquid structures of the s, p-bonded elements shows that this is a somewhat simplistic, but still adequate approximation. In this case the pair potential $\Phi(R)$ and the volume contribution E_1 to the ground-state energy are given by the familiar expressions (we use atomic units and drop the subscript in the pair potential)

$$\Phi(R) = \frac{2Z^2}{R}\left(1 + 16\int_0^\infty \frac{\chi(q)}{\varepsilon(q)}\cos^2(qR_c)\sin(qR)q^{-3}\,\mathrm{d}q\right) \tag{3}$$

$$E_1(n_e) = Z(0.982/R_s^2 - 0.712/R_s + 0.031\ln R_s - 0.115) - E_{ion} \tag{4}$$

$$E_{ion} = 0.5\,\Phi_{ind}(R=0) = 16z^2\int_0^\infty \frac{\chi(q)}{\varepsilon(q)}\cos^2(qR_c)q^{-2}\,\mathrm{d}q \tag{5}$$

where Z is the valence and R_s is the radius of a sphere containing on average one electron. $\chi(q)$ and $\varepsilon(q)$ are the susceptibility and the dielectric function of the electron gas, calculated in the Ichimaru–Utsumi approximation [22]. The core radius $R_c = 1.03$ au has been chosen such as to fit the electronic band structure [20, 21]. In previous optimised random-phase calculations of the structure of liquid Ge [17] it was found that with this value of R_c the interatomic potential describes the structure of liquid Ge rather well.

The interatomic potentials over a wide range of densities are shown in figure 1. At densities close to the equilibrium density of the crystalline phase the potential has a repulsive bump at the nearest-neighbour distance of a hypothetical FCC phase—clearly it will be energetically favourable to form a structure with a lower coordination number, distorting the twelvefold coordinated nearest-neighbour shell as indicated in the figure. Indeed the energy gain from the rearrangement of the nearest-neighbour shell is of the order of the structural energy difference between the FCC and the diamond phases.

Under compression, the Friedel oscillations move inward and the first inflection in $\Phi(R)$ (which is responsible for destabilising the close-packed structures) gradually disappears under the strongly repulsive core and the more compact structures are

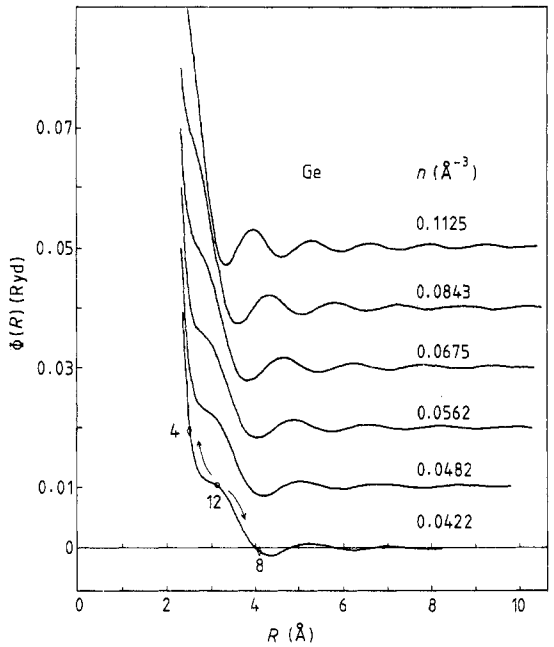

Figure 1. Interatomic pair potential $\Phi(R)$ for Ge as a function of the atomic volume. Under compression, the first oscillation disappears under the repulsive part of the potential, and this drives the trend from an open covalent structure at zero pressure to more close-packed metallic structures with increasing compression (see text).

stabilised. Figure 2 shows the variation of the structural energy differences for a variety of crystal structures relative to the diamond structure. In accordance with experiment [23] we find that the structural sequence is diamond → β-Sn → simple hexagonal (SH). The values for the structural energy differences are in reasonable agreement with those predicted by first-principles calculations [24] (e.g., ΔE (dia − β-Sn) ≃ 0.04–0.05 Ryd/ion at $p = 0$), the predicted transition volume is somewhat too low for the diamond → β-Sn transition, but quite accurate for the β-Sn → SH transition.

Altogether we find that the simple picture of volume and pair forces describes the structural sequence rather well (for earlier second-order pseudopotential calculations of the phase transitions in group IV elements and for a more detailed description see [20, 25, 26]). However we should not forget to mention that only the metallic structures are stable against lattice vibrations when only two-body forces are assumed. In the semiconducting diamond structure three-body forces are necessary to stabilise the low-lying transverse acoustic modes.

3. Molecular dynamics

The simulations of liquid Ge were carried out for a classical (N, V, E) MD ensemble in a cubic box subject to periodic boundaries. The Newtonian equations of motions were integrated using a fourth-order predictor–corrector algorithm in the Nordsieck formulation [27–29] with one iteration in the corrector step. This algorithm is very suitable for MD calculations and allows larger time increments than the simpler Verlet algorithm

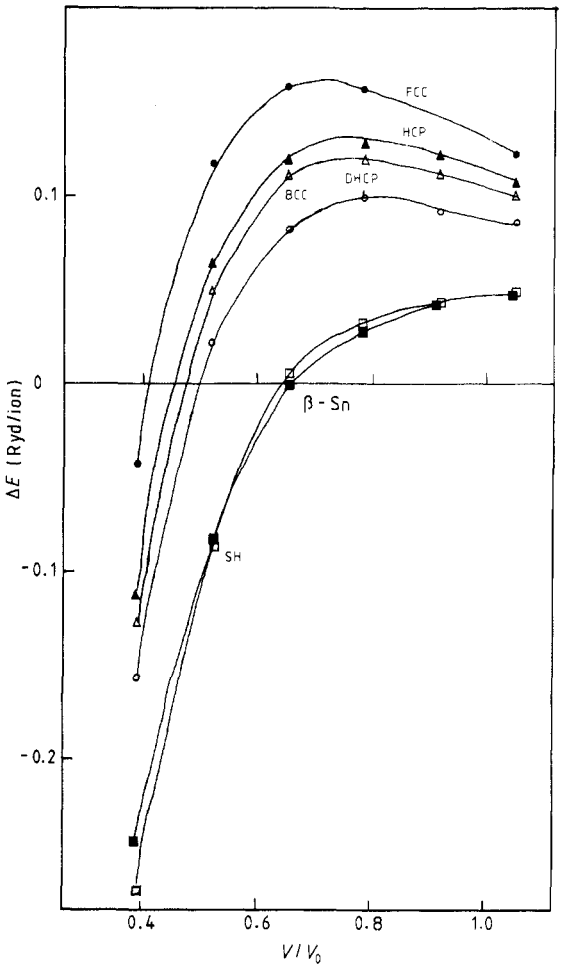

Figure 2. Structural energy differences ΔE in Ge, relative to the diamond structure: ■, β-tin; □, simple hexagonal; ▲, hexagonal-close-packed; Δ, double hexagonal-close-packed; ○, body-centred cubic; ●, face-centred cubic.

[30–32]. With a time step of 0.3×10^{-14} s the total energy remained constant to four significant figures during the production runs.

The calculations were performed for a system of $N = 1372$ atoms. Parallel runs for smaller systems (down to 60 atoms) served to check the system size dependence, with a view of creating smaller ensembles which could serve as a basis for electronic structure calculations [33]. The structure (i.e. $g(r)$) was found to be insensitive to a change in the system size up to distances where the periodic boundaries became apparent.

In order to take into account the Friedel oscillations, the pair potential was cut off at 10.4 Å, a relatively large value which means 32.9% of the length of the edge of the MD cell 31.6 Å. In the rather large MD ensemble we thus obtained a reliable pair correlation function on a range up to 15.8 Å, which in turn provided a smooth structure factor $S(q)$, even in the small-angle region.

This cut-off radius leads to an interaction of each particle with an average of 200 neighbours. To find out these next neighbours in each MD step we developed a method we call 'net-cube approximation of the cut-off sphere': the MD cell is broken into 6^3–16^3 (or more) identically sized net cubes, with a length of the edge down to a third of the cut-off radius. Only net cubes with a non-empty intersection with the cut-off sphere are considered. This way, a construction of 13–155 net cubes emerges, which is related to the ratio of lengths and the relative position of the actual central particle in its net cube. The particles contained in each net cube are stored in a linked list, which is updated for every time step. The time-optimised realisation of this idea is rather complicated, but for larger numbers of particles it is very effective: the computational time increases linearly with N, the storage requirement is completely independent of the cut-off radius and updating is not performed in intervals of some MD steps only. Some effort was also spent on an accurate numerical realisation of the Fourier transform from the pair correlation function $g(R)$ to the static structure factor $S(q)$. Our method uses the 'raw data' from the MD simulation only, without any extrapolation to large values of R. Some new ideas to improve the accuracy of $S(q)$ for small momentum transfers have been implemented.

(i) Optimal choice of the cut-off R_{max} (which means that we do not necessarily use the full set of $g(R)$ data).

(ii) The discrete $g(R)$ values should be assigned to the centre of the interval over which the distances have been sampled.

(iii) Calculation of $S(q)$ for more than the classical arguments obtained by fast Fourier transforms.

A detailed description of the various new technical aspects together with interesting parts of the code will be published elsewhere [29].

The simulation started with the atoms arranged in an ideal FCC lattice. This choice was arbitrary in so far as the equilibrated liquid is independent of the initial configuration. The behaviour at the beginning of the simulation, of course, depends heavily on the lattice used.

In the first run the system was molten at 1570 K. As a rule of thumb 'melting' was observed by means of the melting factor [28]. The initial temperature drifts were adjusted by scaling both velocities and third derivatives (for consistency of the system of differential equations) by a common factor; in the same way the temperature was varied between the different production runs.

In the second run 2500 steps were calculated to reach equilibrium. The production runs took 600 time steps (1.8 ps), with $g(r)$ simultaneously calculated. Equilibrium was controlled by comparing several successive plots of $g(r)$ based on 20 configurations and by observing temperature. The resulting data is an average of 100 configurations.

After the production, the temperature was lowered by a slow-cooling process (reduction less than 0.9 K/step) and another 550 steps were calculated to equilibrate the system at the new temperature. This procedure was repeated several times down to 650 K.

After calculations for the highest density considered ($n = 0.0465$ Å^{-3}, $\rho = 5.650$ g cm^{-3}), we expanded the system and introduced the pair potential corresponding to the next lower density ($n = 0.0457$ Å^{-3}). The calculations for this density, which did not serve for data in this paper, were used to increase temperature up to 1570 K, so that the next density could be treated like the first one.

The entire procedure was repeated for several different densities.

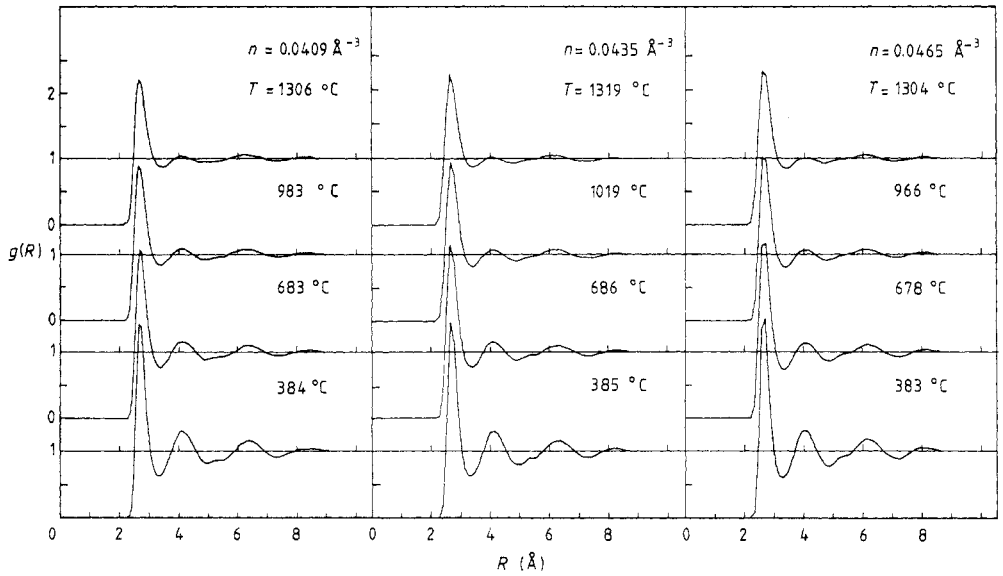

Figure 3. Pair correlation function $g(R)$ of liquid and super-cooled liquid Ge as a function of temperature and density.

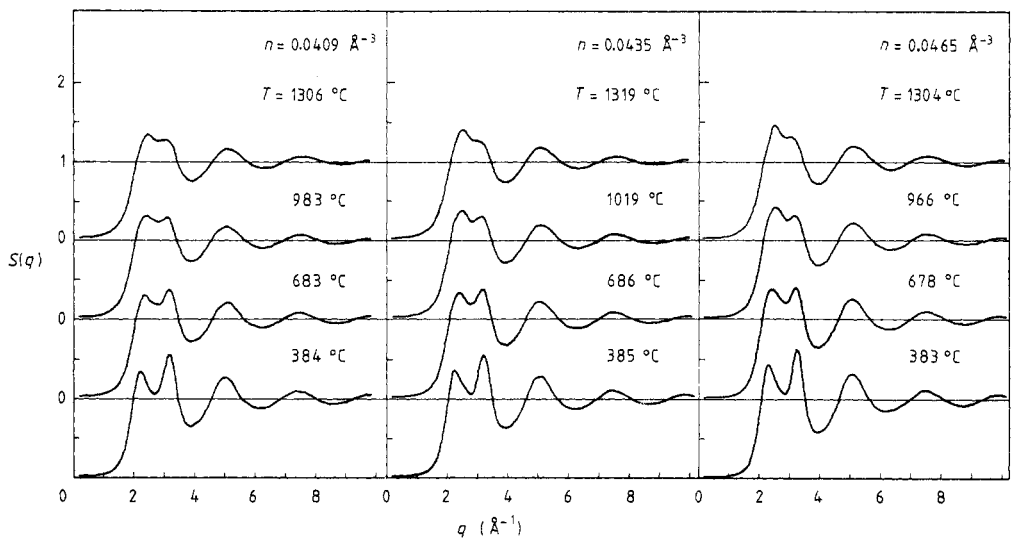

Figure 4. Static structure factor $S(q)$ of liquid and supercooled liquid Ge as a function of temperature and density.

4. Structure of liquid germanium

The pair correlation functions and static structure factors for Ge at various temperatures including the liquid and supercooled liquid regimes are shown in figures 3 and 4. The

correlation functions are very different from those of a normal liquid metal: if R_1 is the position of the first peak in $g(R)$, the second peak is usually found at 1.85–$1.90R_1$ (see, e.g., Waseda [34]). In liquid Ge the second peak is shifted to $2.25R_1$, and an intermediate peak has appeared at $1.6R_1$. The position of this peak corresponds exactly to the position of the first minimum in the effective pair interaction (cf figure 1), and the shift of the second peak is also seen to follow the attractive minimum of the pair potential. Altogether the complex structure of liquid Ge is found to result from the interplay of the geometrical requirements of sphere packing and of the intermediate and long-range oscillatory potential. The position of the first peak is set by the diameter of the repulsive core of the Ge pseudoatom, $\sigma \simeq 2.72$ Å. The more distant peaks are set by the oscillations of the pair potential, they appear at distances equal to the Friedel wavelength $\lambda_F = 2\pi/2k_F \simeq 1.82$ Å. Only a weak shoulder at the left-hand side of the third peak appears at the distance where one would expect the second peak of the correlation function of a liquid described in terms of soft-sphere packing. For distances larger than 10 Å, the interference of the oscillations with different wavelengths (σ and λ_F) leads to very rapid damping of the oscillations in the correlation functions.

These arguments are also corroborated by the form of the static structure factor: the main peak appears at $Q_1 \simeq 2\pi/\sigma = 2.3$ Å^{-1}, with a shoulder at $Q_s \simeq 2\pi/\lambda_F = 2k_F = 3.4$ Å^{-1}. Such a correlation between the shoulder in the structure factor and the Fermi wavevector in complex polyvalent liquid metals was first pointed out by Beck and Oberle [35], see also [17, 18]. Let us note that the amplitude of the shoulder in the structure factor is rather sensitive to the cut-off radius in the potential. If a cut-off radius smaller than 10 Å is used, the shoulder is sensibly weaker.

The comparison of the MD results with x-ray and neutron diffraction data is complicated by the fact that the agreement between the different experiments is far from perfect. For the pair correlation function we find a reasonable agreement with the combined experimental data (figure 5(*a*)). In the structure factor we observe a tendency to overestimate the shoulder at the expense of the main peak—i.e., the $2k_F$—correlations relative to the packing correlations (figure 5(*b*)). However, these are precisely the points where the scatter in the experimental data is largest.

The nearest-neighbour coordination number may be calculated by integrating over the first peak of the correlation function. Unfortunately, there is no general agreement as to how precisely this integration should be performed: (i) integration over the radial distribution function up to the position of R_{min} of the first minimum in $g(R)$ (see figure 3), (ii) integration up to R_{max}, multiplied by two (i.e. integration over the symmetric part of the first peak), or (iii) integration over a Gaussian fitted to the first peak. The largest coordination number generally follows from method (i). The results are very sensitive to the precise value of R_{min}, varying R_{min} by ± 0.126 Å (this is the width of the interval used for the calculation of the correlation function) changes N_c on average by ± 0.4. At $T = 980$ °C we find $N_c = 7.6$, slightly larger than the values derived from the diffraction data: $N_c = 6.5$ (calculated using method (ii) [3]), $N_c = 6.8$ [2], $N_c = 6.7$ [5], $N_c = 7.1$ [36] (the method used to calculate N_c is not specified). With falling temperature and decreasing density we find a pronounced decrease of the coordination number (table 1).

Here it is interesting to make a comparison between the MD results and our earlier calculations of the structure of liquid Ge using the optimised random-phase approximation (ORPA), based upon the same interatomic potential [17] (figure 6). We find a good agreement in general, but again the packing correlations are more expressed in the ORPA. The difference between the MD and the ORPA is easily understood: the ORPA is a perturbative method. Starting from a hard-sphere reference fluid, corrections for

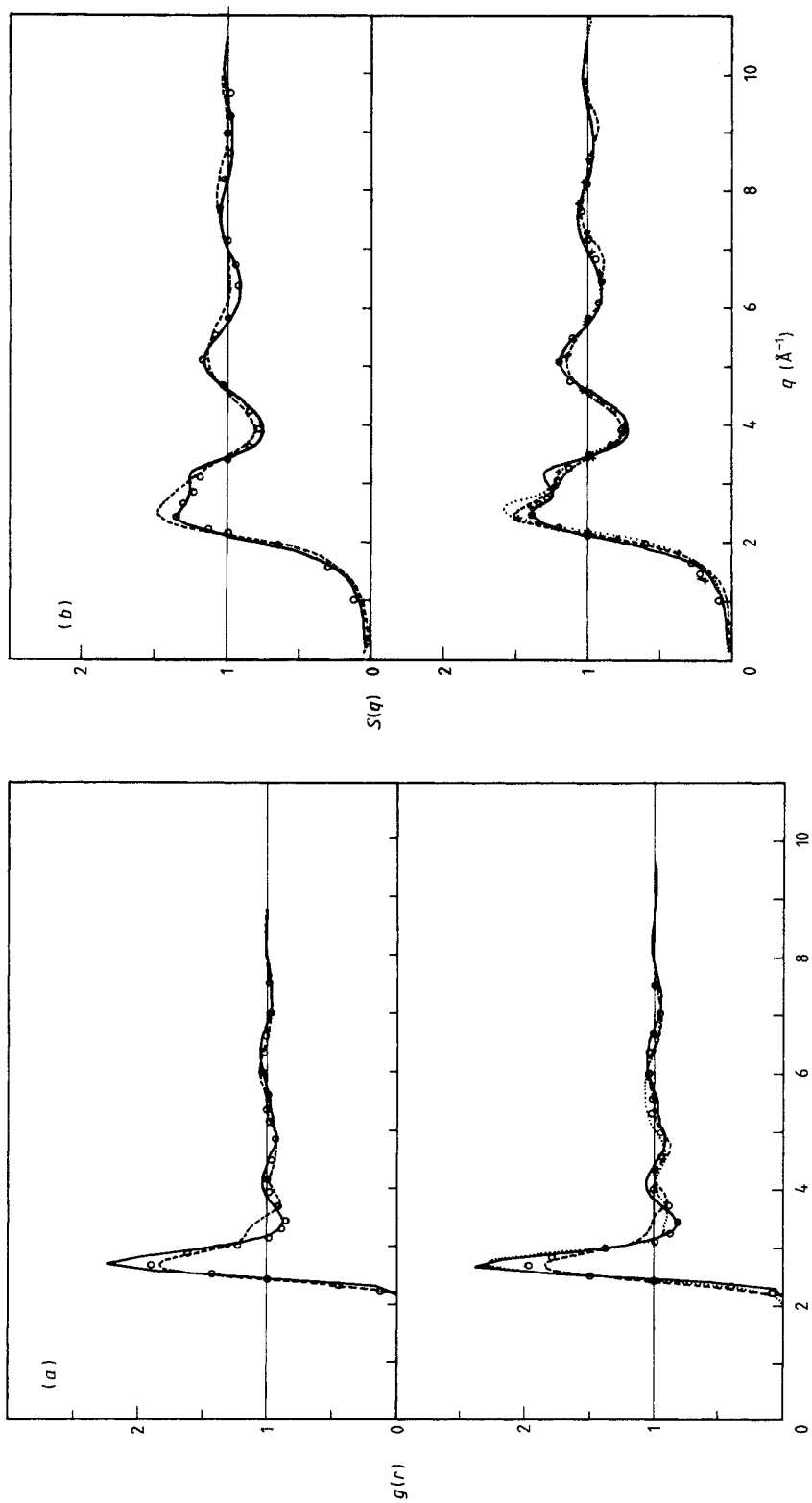

Figure 5. Comparison between MD simulations (full curves) and experimental data for (*a*) pair correlation function and (*b*) structure factor. The experimental data are from Gabathuler and Steeb [3] (neutron diffraction, broken curve), Waseda and Suzuki [2] (x-ray diffraction, dotted curve), Bellisent-Funel and Bellisent [5] (neutron diffraction, open circles) and Davidovic *et al* [4] (neutron diffraction, crosses). (*a*) Top panel: ——, MD, $T = 1308$ °C; – – –, expt 1, $T = 1300$ °C; open circles, expt 3, $T = 1200$ °C. Bottom panel: ——, MD, $T = 1019$ °C; – – –, expt 1, $T = 960$ °C; · · · · ·, expt 2, $T = 980$ °C; open circles, expt 3, $T = 950$ °C. (*b*) Top panel: ——, MD, $T = 1308$ °C; – – –, expt 1, $T = 1300$ °C; open circles, expt 3, $T = 1200$ °C. Bottom panel: ——, MD, $T = 1019$ °C; – – –, expt 1, $T = 960$ °C; · · · · ·, expt 2, $T = 980$ °C; open circles, expt 3, $T = 950$ °C; crosses, expt 4, $T = 850$ °C.

Table 1. Nearest-neighbour coordination number N_c in liquid and supercooled liquid Ge.

T (°C) / n (Å^{-3})	1310	980	680	383
0.0465	8.4	8.1	7.5	7.2
0.0450	8.2	8.0	7.4	7.1
0.0435	7.7	7.6	7.3	6.5
0.0422	7.6	7.5	6.9	6.4
0.0409	7.0	6.8	6.5	5.9

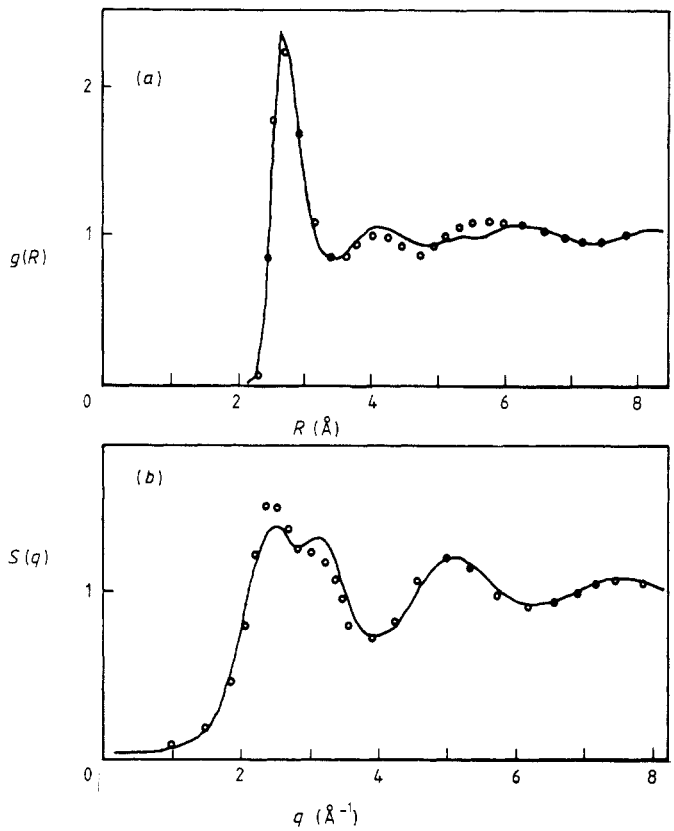

Figure 6. Comparison between the MD simulation (full curves) and the optimised random phase approximation (OPRA) [17, 18] (open circles).

the softness of the repulsive interactions and for the long-range oscillatory interactions are added in a perturbation approach. Thus the packing correlations are very strong, and it seems that the perturbation calculation does not account for the full effect of the oscillatory interactions.

The explanation of the difference between MD and experiment is more difficult. As the calculations overestimate the differences between Ge and a 'normal' liquid metal, it is not likely that the missing three-body forces are responsible for the difference. On the other hand it is known that at these high temperatures the mean free path of the electrons

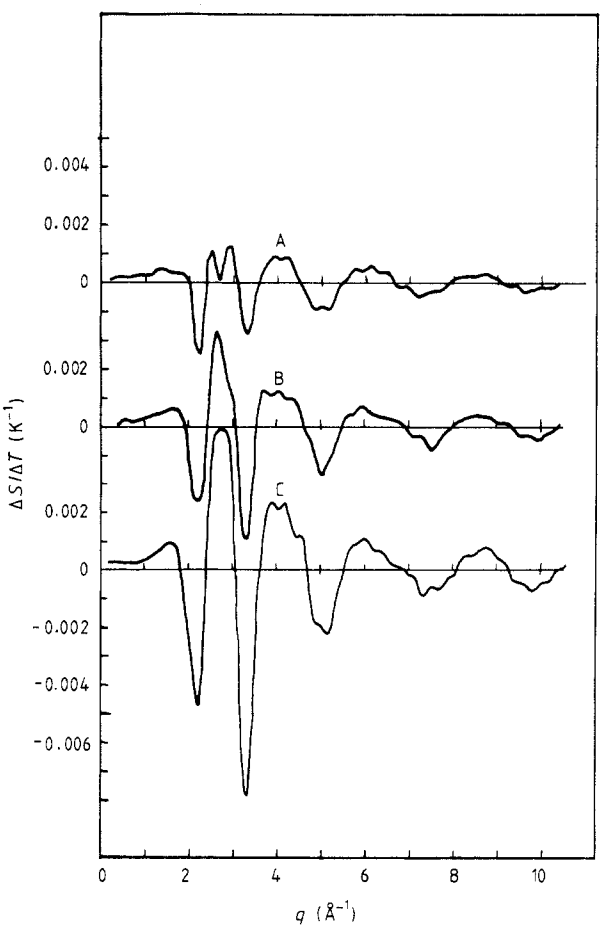

Figure 7. Temperature derivative of the static structure factor $\partial S(q)/\partial T$ in liquid and supercooled liquid Ge. The differential $\partial S(q)/\partial T$ is approximated by the quotient $\Delta S(q)/\Delta T$, $T = T_1 - T_2$. Curve A: $T_1 = 1295\,°C$, $T_2 = 965\,°C$; curve B: $T_1 = 965\,°C$, $T_2 = 678\,°C$; curve C: $T_1 = 678\,°C$; $T_2 = 382\,°C$, $n = 0.0435$, $\Delta T = T_1 - T_2$.

is finite, and that a finite mean free path yields to a smearing out of the Fermi surface singularity in the screening function and a damping of the Friedel oscillations in the interatomic potentials [37, 38].

4.1. Temperature dependence of the structure of liquid germanium

The structure of liquid Ge is strongly dependent on temperature (figures 3 and 4). This is most distinctly expressed in the structure factors: at lower T the shoulder in $S(q)$ becomes a separate peak, and in supercooled liquid Ge, the intensity is even larger than that of the first peak (figure 7). Thus supercooled liquid Ge has a structure approaching amorphous Ge [39, 40]. However, the coordination number is still $N_c \simeq 6.5$, a quench to very low temperatures would result not in a semiconducting a-Ge, but in a metallic amorphous form (which can be produced in the laboratory only by applying pressure [7]).

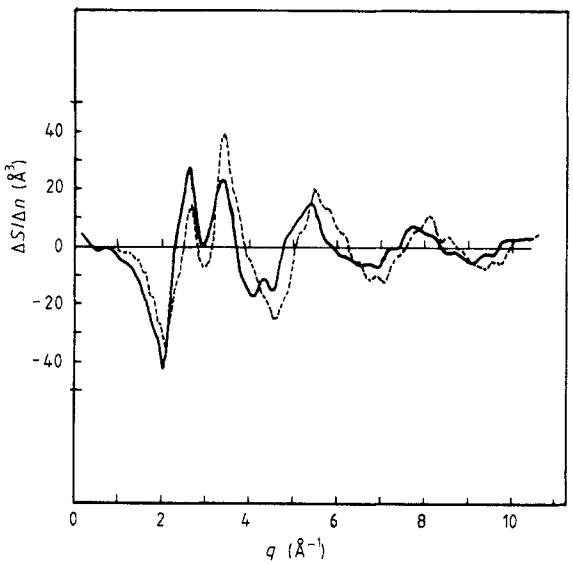

Figure 8. Density derivative $\partial S(q)/\partial n \simeq \Delta S(q)/\Delta n$, $\Delta n = n_1 - n_2$ of the static structure factor of liquid Ge at $T = 990\,^{\circ}\mathrm{C}$ and $n = 0.0435\ \text{Å}^{-3}$, $n_1 = 0.0450\ \text{Å}^{-3}$ ($T_1 = 994\,^{\circ}\mathrm{C}$), $n_2 = 0.0422\ \text{Å}^{-3}$ ($T_2 = 989\,^{\circ}\mathrm{C}$) (full curve), compared with the prediction of the uniform fluid model $\partial S(q)/\partial n = -(q/3n)(\partial S(q)/\partial q)$ with $n = 0.0435\ \text{Å}^{-3}$, $T = 1019\,^{\circ}\mathrm{C}$ (broken curve).

The temperature variation of $S(q)$ is strongly non-linear, demonstrating that the ordering effects increase progressively with falling temperature. This should also be reflected in the thermodynamic functions: we expect that the specific heat should increase with the degree of undercooling: From our MD results we find $C_v \simeq 19.5\ \text{J mol}^{-1}\,\text{K}^{-1}$ at $T \simeq 1170\,^{\circ}\mathrm{C}$, $C_v \simeq 21\ \text{J mol}^{-1}\,\text{K}^{-1}$ at $T \simeq 733\,^{\circ}\mathrm{C}$, and $C_v \simeq 25\ \text{J mol}^{-1}\,\text{K}^{-1}$ at $T \simeq 533\,^{\circ}\mathrm{C}$. The last two values refer to a supercooled liquid. Such a behaviour of the specific heat has indeed been observed in supercooled polyvalent liquid metals [41].

4.2. Density dependence of the structure of liquid Ge

For most normal liquid metals, the density dependence of the static structure factor is well described by the uniform fluid model [42, 43], i.e. one has

$$\frac{\partial S(q)}{\partial n} = -\frac{n}{3q}\frac{\partial S(q)}{\partial q}. \tag{6}$$

Equation (6) expresses the fact that the variation of the liquid structure with density is essentially restricted to a scaling of all interatomic distances proportional to $q^{-1/3}$. Figure 8 shows that in liquid Ge there are some characteristic deviations from the uniform fluid model which reflect the density dependence of the interatomic potentials:

(i) the intensity ratio of the two first peaks is inverted (figure 8). Under compression, the geometrical packing effects become more important than predicted by the uniform fluid model, in agreement with the variation of the pair potential shown in figure 1.

(ii) The phase difference between $\partial S(q)/\partial n$ and the prediction of the uniform fluid model at larger momentum transfers shows that the outward shift of the oscillations in $S(q)$ under compression is smaller than predicted by the simple scaling law (6)—again

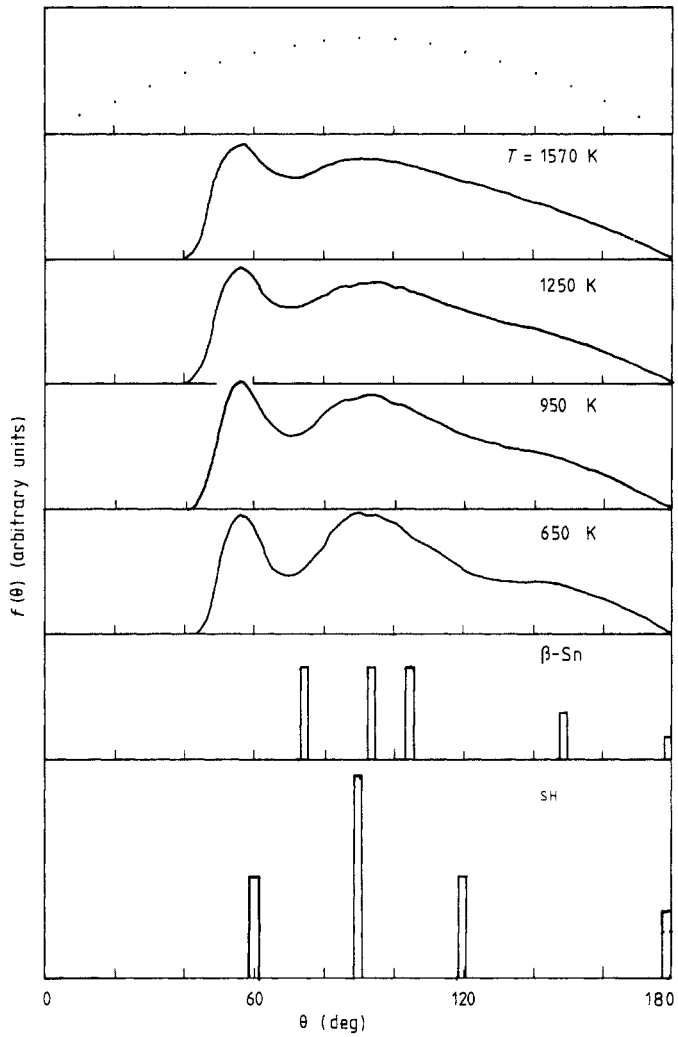

Figure 9. Bond-angle distribution function $f(\theta)$ for liquid and supercooled liquid Ge. The distribution of the bond angles in the metallic high-pressure polymorphs with the β-tin and the simple hexagonal structure is given for comparison. The dotted curve at the top shows the sinusoidal random distribution.

this reflects the increase of the effective diameter of the Ge atoms under compression (see figure 1).

4.3. Beyond pair correlations

A possibility to characterise the local order in a liquid beyond the level of a pair correlation function is to consider the bond-angle distribution function $f(\theta)$: $f(\theta)$ gives the probability of finding an angle between triplets of particles, the lengths of the bonds including the angle being both less than the position of the first minimum in the correlation function (figure 9). In liquid Ge we find a double-peaked bond-angle distribution, in the undercooled liquid a shoulder develops at $\theta \simeq 140°$. The maximum

at $\theta \simeq 90°$ and the position of the shoulder correlate rather well with the bond-angles in the metallic β-tin phase of Ge, but the bond angles at $\theta \simeq 60°$ (corresponding to nearest-neighbour triplets) are found only in the simple hexagonal high-pressure phase.

Bond-angle distributions calculated from models based on parametrised two- and three-body forces show that the parametrisations are far from unique. With the Biswas–Hamann potential function [7] Biswas *et al* [13] calculate a $f(\theta)$ similar to ours, with a peak near $\theta \simeq 60°$ and a second one somewhat closer to the tetrahedral angle. This form of $f(\theta)$ is obtained even in a liquid quenched to room temperature. On the other hand Broughton and Li [11] find a bond-angle distribution where the 60° peak is absent even in the liquid state. Their calculation is based upon the Stillinger–Weber [9] potential function. Both potential functions involve a three-body term which minimises the energy of the triplet for a tetrahedral bond angle, but still yield very different bond angle distributions. In both papers the authors note that the driving force to amorphisation out of the liquid is very small. Amorphisation (i.e. transition to a four-coordinated disordered structure) occurs only if the three-body terms are multiplied arbitrarily by a factor of at least 2.5 [13]. This supports the argument brought forward in the introduction that the interatomic forces in Ge are strongly state-dependent.

Our results confirm the conclusions drawn on the basis of these results that the quenching of liquid Si and Ge does not lead to a glass-transition associated with a metal–semiconductor transition unless the changes in the interatomic interactions accompanying the transitions are taken into account.

5. Conclusions

We have presented a molecular dynamical investigation of the structure of liquid and supercooled liquid Ge. We find that the complex structure of liquid Ge is well described in terms of volume- and density-dependent pair forces, without any adjustable parameter. Structure factor and pair correlation function agree well with experimental data—in fact better than for most computer-simulations based on parametrised two- and three-body forces (see, e.g., [12]). The characteristic liquid structure arises from the interplay of two characteristic distances, the diameter of the repulsive core and the Friedel wavelength of the oscillations in the interatomic potentials.

The density dependence of the structure shows a marked deviation from the uniform fluid model, arising from the density dependence of the interatomic potentials.

The structure varies strongly with temperature. The non-linear increase of the ordering effects with progressive undercooling leads to an increasing specific heat, as observed in many supercooled polyvalent metals.

The bond-angle distribution function shows that the local order in liquid Ge is different from that in both the semiconducting and the metallic solid phase. This is also supported by the electronic structure. The electronic density of states of liquid Ge is distinctly different from that of the α-Ge and β-Ge phases, and far from a free-electron form [44]. Electronic structure calculations based on the present MD model for liquid Ge are in good agreement with recent photoemission data—results will be published soon [33].

The structure of undercooled liquid Ge does not tend towards the structure of amorphous Ge—in agreement with computer simulations based on parametrised potential energy functions. This shows that a proper description of the metal–semiconduction transition accompanying solidification is possible only with state-dependent interatomic

forces. Not only do the effective two-body forces change with electron density, but with a decreasing coordination number the contribution of an sp^3-type hybridisation to the electronic density of states and hence three-body forces will become much more important than in the equilibrium liquid.

Acknowledgments

Partial financial support from the Fonds zur Förderung der wissenschaftlichen Forschung (Austrian Science Foundation) under Project no. 6191 is gratefully acknowledged.

References

[1] Glazov V M, Chizhevskaya S N and Glagoleva N N 1969 *Liquid Semiconductors* (New York: Plenum) ch 3
[2] Waseda Y and Suzuki K 1975 *Z. Phys.* B **20** 339
[3] Gabathuler J P and Steeb S 1979 *Z. Naturf.* a **34** 1314
[4] Davidovic M, Stojic M and Jovic D 1983 *J. Phys. C: Solid State Phys.* **16** 2053
[5] Bellisent-Funel M C and Bellisent R 1984 *J. Non-Cryst. Solids* **65** 383
[6] Bergman C, Bichara C, Chieux P and Gaspard J P 1985 *J. Physique Coll.* **46** C8 97
[7] Shimomura O, Minomura S, Sakai N, Asamuni K, Tamura K, Fukushima J and Endo H 1974 *Phil. Mag.* **32** 547
[8] Stillinger F H and Weber T A 1985 *Phys. Rev.* B **31** 5262
[9] Tersoff J 1986 *Phys. Rev. Lett.* **56** 632
[10] Biswas R and Hamann D 1985 *Phys. Rev. Lett.* **55** 2001; 1987 *Phys. Rev.* B **36** 6434
[11] Broughton J Q and Li X P 1987 *Phys. Rev.* B **35** 9120
[12] Kluge M D, Ray J D and Rahman A 1987 *Phys. Rev.* B **36** 4234
[13] Biswas R, Grest G S and Soukolis C M 1987 *Phys. Rev.* B **36** 7437
[14] Ding K and Andersen H C 1986 *Phys. Rev.* B **34** 6987
[15] Car R and Parrinello M 1987 *Proc. 18th Int. Conf. Physics of Semiconductors* ed. O Engstrom (Singapore: World Scientific) p 1165
[16] Car R and Parrinello M 1988 *Phys. Rev. Lett.* **60** 204
[17] Kahl G and Hafner J 1984 *Solid State Commun.* **49** 1125
[18] Hafner J and Kahl G 1984 *J. Phys. F: Met. Phys.* **14** 2259
[19] Pettifor D G 1983 *Physical Metallurgy* vol 1, ed. R W Cahn and P Haasen (North Holland: Amsterdam) ch 3
[20] Hafner J 1987 *From Hamiltonians to Phase Diagrams, Springer Series in Solid State Sciences* vol 70 (Berlin: Springer)
[21] Hafner J and Heine V 1983 *J. Phys. F: Met. Phys.* **13** 2479; 1986 *J. Phys. F: Met. Phys.* **16** 1429
[22] Ichimaru S and Utsumi K 1981 *Phys. Rev.* B **24** 7385
Ichimaru S 1982 *Rev. Mod. Phys.* **54** 1017
[23] Olijnyk H, Sikka S K and Holzapfel W B 1984 *Phys. Lett.* **103A** 137
[24] Chang K J and Cohen M L 1986 *Phys. Rev.* B **34** 8581
[25] Hafner J 1974 *Phys. Rev.* B **10** 4151
[26] Soma T 1978 *J. Phys. C: Solid State Phys.* **11** 2669
[27] Gear C W 1971 *Numerical Initial Value Problems in Ordinary Differential Equations* (Englewood Cliffs, NJ: Prentice Hall) chs 9, 10
[28] Vesely F 1978 *Computerexperimente an Flüssigkeitsmodellen* (Weinheim: Physik) chs 3.2.3
[29] Arnold A, Mauser N and Hafner J 1988 *Comp. Phys. Commun.* submitted for publication
[30] Beeman D 1976 *J. Comp. Phys.* **20** 130
[31] Venneri G D and Hoover W G 1987 *J. Comp. Phys.* **73** 468
[32] Toxvaerd S 1983 *J. Comp. Phys.* **20** 214
[33] Jank W and Hafner J 1988 *Europhys. Lett.* **7** 623
[34] Waseda Y 1981 *The Structure of Non-Crystalline Materials—Liquids and Amorphous Solids* (New York: McGraw-Hill)

[35] Beck H and Oberle R 1980 *J. Physique Coll.* **40** C8 289
[36] Isherwood S P, Orton B R and Manaila R 1972 *J. Non-Cryst. Solids* **8** 691
[37] de Gennes P 1962 *J. Physique* **23** 630
[38] Takanaka K and Yamamoto R 1977 *Phys. Status Solidi* b **84** 813
[39] Graczyk J F and Chaudhari P 1973 *Phys. Status Solidi* b **58** 601
[40] Paasche F, Olbrich H, Schestag U, Lamparter P and Steeb S 1982 *Z. Naturf.* a **37** 1139
[41] Perepezko J H and Paik J S 1984 *J. Non-Cryst. Solids* **61+62** 113
[42] Egelstaff P A and Wang S S 1972 *Can. J. Phys.* **50** 2451
Egelstaff P A, Suck J B, Gläser W, McPherson R and Teitsma A 1986 *J. Physique Coll.* **40** C8 222
[43] Kahl G and Hafner J 1985 *Z. Phys.* B **58** 283
[44] Indlekofer G, Oelhafen P, Lapka R and Güntherodt H J 1988 *Z. Phys. Chem.* **157** 465
Indlekofer G 1988 *PhD Thesis* University of Basel